Very High-Frequency Radar Mapping of Surface Currents

Lynn K. Shay, Thomas M. Cook, Hartmut Peters, Arthur J. Mariano, Robert Weisberg, P. Edgar An, Alexander Soloviev, and Mark Luther

***Abstract*—An ocean surface current radar (OSCR) in the very high frequency (VHF) mode was deployed in South Florida Ocean Measurement Center (SFOMC) during the summer of 1999. During this period, a 29-d continuous time series of vector surface currents was acquired starting on 9 July 1999 and ending 7 August 1999. Over a 20-min sample interval, the VHF radar mapped coastal ocean currents over a 7.5 km $\times$ 8 km domain with a horizontal resolution of 250 m at 700 grid points. A total of 2078 snapshots of the two-dimensional current vectors were acquired during this time series and of these samples, only 69 samples (3.3%) were missing from the time series. During this period, complex surface circulation patterns were observed that included coherent, submesoscale vortices with diameters of 2 to 3 km inshore of the Florida Current. Comparisons to subsurface measurements from moored and ship-board acoustic Doppler current profiles revealed regression slopes of close to unity with biases ranging from 4 to 8 cm s^{-1} between surface and subsurface measurements at 3 to 4 m beneath the surface. Correlation coefficients were 0.8 or above with phases of -10 to -20° suggestive of an anticylconic veering of current with depth relative to the surface current. The radar-derived surface current field provided spatial context for an observational network using mooring-, ship- and autonomous underwater vehicle-sensor packages that were deployed at the SFOMC.**

***Index Terms*—ADCP, coastal ocean circulation, current profiles, surface currents, VHF radar, vortices.**

I. Introduction

ACCURATE measurement of ocean surface currents has been one of the more elusive phenomena to confront ocean scientists. Given increased national attention to the coastal ocean and in the planned networking of coastal ocean observatories, the acquisition of the highest quality surface current data is required to provide spatial context for the emerging suites of *in situ* instrumentation. Furthermore, long-term monitoring of the surface circulation would provide important data to study its impact on societally relevant issues such as search and rescue operations, coastal pollution from sewage plants, transport of harmful algae blooms, oil spills and its mitigation, beach erosion and renourishment, and air–sea interaction studies.

One of the more promising techniques that has evolved over the past four decades is the Doppler radar technique [1]. Radar signals are backscattered from the moving ocean surface by resonant surface waves of one-half the incident radar wavelength. This Bragg scattering effect results in two discrete peaks in the Doppler spectrum [2]. In the absence of a surface current, spectral peaks are symmetric about the Bragg frequency (ν_b) offset from the origin by an amount proportional to $2c_o\lambda^{-1}$, where c_o represents the linear phase speed of the surface wave and λ is the radar wavelength. If there is an underlying surface current, Bragg peaks in the Doppler spectra are displaced by an amount of $\Delta\nu = 2V_{cr}\lambda^{-1}$, where V_{cr} is the radial component of current along the direction of the radar. Thus, to resolve the two-dimensional (2-D) current fields, two radar stations are required where their separation determines the domain of the mapped region. While the accuracy of the measurement is a maximum for an angle of intersection of 90° between the two radar beams, the error in resolving the current vectors increases as the intersection angle departs from this optimal value.

The concept of using high frequency (HF) and very high frequency (VHF) radar pulses to probe ocean surface currents has received considerable attention in coastal oceanographic experiments in Europe and the United States [3], [4]. The two systems that have been used are the Coastal Ocean Dynamics Applications Radar (CODAR) [5] and the Ocean Surface Current Radar (OSCR) [6], [7]. More recently, a WEllen RAdar (WERA) system has been developed that also utilizes phased-array technology [8]. While all these systems are based on resonant Bragg backscatter, there is a fundamental difference in the methodology used to isolate the ocean area where scattering occurs. The OSCR system utilizes an 85-m-long 16- (HF) or 32- (VHF) element phased-array antennae to achieve a narrow beam, electronically steered over the illuminated ocean area (Table I). The beamwidth is a function of the radar wavelength divided by the length of the phased array, which is 7° for the HF mode and 3.5° for VHF mode. By contrast, CODAR utilizes a three-element crossed-loop/monopole antennae system and direction-finding techniques that are easily deployed in small, confined areas compared to the beach real estate required for the length of the phased array. The azimuthal resolution of the current field is based on a least-squares fit of the Fourier series to the data [9]. Thus, the current resolution tends to be more sensitive to beam patterns in direction-finding algorithms.

In a comprehensive review of the HF radar issues [3], theoretical and observed beam patterns were compared for a 16-element

Manuscript received December 18, 2000; revised October 15, 2001. This work was supported by the Ocean Modeling Program under Grant N00014-98-1-0818.

L. K. Shay, T. M. Cook, H. Peters and A. J. Mariano are with the Division of Meteorology and Physical Oceanography, Rosenstiel School of Marine and Atmospheric Science, University of Miami, Miami, FL 33149 USA (e-mail: nick@iwave.rsmas.miami.edu).

R. Weisberg and M. Luther are with the Department of Marine Science, University of South Florida, St. Petersburg, FL 33701 USA.

P. E. An is with the Division of Ocean Engineering, Florida Atlantic University, Dania Beach, FL 33004 USA.

A. Soloviev is with the Department of Oceanography, NOVA Southeastern University, Dania Beach, FL 33004 USA.

Publisher Item Identifier S 0364-9059(02)03374-5.

phased array. For a beam steered at 22° relative to the phased array, observed side lobes in the beam pattern were typically 20–25 dB less than theoretical side lobes in the beam pattern. Observed and theoretical peaks were equal at 22°, suggesting that the surface current measurements were well resolved. As all HF-radar antennae systems have a characteristic beam pattern, environmental factors such as salinity and moisture and path length from the antennae to the sea influence the beam pattern. In addition, for larger phased arrays, the beach terrain may under some conditions constrain the angle of the boresite, which directly impacts the beam intersection angles and the resolution of the surface current vector. Within this framework, phased array systems (i.e., OSCR, WERA) to measure surface currents tend to be more hardware intensive whereas crossed-looped monopole antennae systems (i.e., CODAR) requires more software manipulations to determine current speed and direction.

While HF-radar techniques to measure surface currents have existed for several years, little attention has focused on the comparisons to conventional oceanographic measurement techniques, except for tidal bands [6], [10]. Recently, surface currents have been compared to subsurface currents from both fixed and moving platforms during a series of experiments using phased-array technology [7], [11]–[14]. Point-by-point comparisons have revealed both similarities and differences between surface and subsurface current signals. For example, rms differences have ranged between 7 to 15 cm·s^{-1} depending on the depth of the subsurface measurement. In the NSF and ONR sponsored *Duck94* experiment, comparisons to a vector measuring current meter (VMCM) at 4 m beneath the surface indicated an rms difference of 7 cm·s^{-1} over a range of 1 m·s^{-1} current from a 29-d time series. Given the VMCM's measurement accuracy of about 2 cm·s^{-1}[15], the accuracy for the surface currents was about 5 cm·s^{-1}, consistent with the manufacturer's cited values (see Table I). Although differences still remain, radar-derived surface current measurements represent the integral of currents in the top meter (or less) of the water column ($\lambda/8\pi$) [2] where winds and waves impact surface currents and near-surface shears. An important issue emerging from recent radar studies is that mooring data represents a point measurement whereas radar-derived estimates are averaged over areas with dimensions of 0.6 to 4 km^2 for the VHF and HF radars, respectively.

In the VHF mode ($\approx$ 49.95 MHz), comparisons to subsurface measurements have been generally lacking due in part to its under utilization in coastal experimentation. In the VHF mode of OSCR, the radar wavelength is 5.9 m corresponding to a Bragg wavelength of 2.95 m. The highest spatial resolution for this mode is 250 m, which makes the use of VHF radar particularly attractive for bays and ports as well as monitoring surface circulation around sewage effluent regions [16]. Measurements from a 3-month deployment of a VHF profiler in the equatorial Pacific Ocean revealed complex surface current patterns that contained both short- and long-time scale variability [17]. Recent surface current observations using VHF radar revealed complex surface current patterns in the South Florida Ocean Measurement Center (SFOMC) where coherent, submesoscale vortices had diameters of 2 to 3 km just inshore of the Florida Current (FC) [18]. These high-resolution surface current observations provided spatial context for autonomous underwater vehicles (AUVs), a series of upward-looking acoustic Doppler current profiler (ADCP) from moorings and ship-based ADCP and conductivity-temperature-depth (CTD) measurements (Fig. 1). This experimental approach provided a multiple-scale nesting of relevant submesoscale variability in a coastal ocean subject to large relative vorticity changes across the shelf break associated with FC intrusions [19]. The longer-term significance of this approach provides a strategy for coastal ocean studies for the planned networking of observatories using emerging measurement technologies.

TABLE I
RSMAS OSCR SYSTEM CAPABILITIES AND SPECIFICATIONSFOR THE VHF MODE

Number of measurement cells	700
Operation range (km from radar site)	11
Range cell resolution (km)	0.25
Measurement depth (m)	0.2
Measurement cycle (min)	20
Cited Accuracy:	
Radial current (cm s $^{-1}$)	2
Vector curent (cm s $^{-1}$)	4
Vector direction (°)	5
Data Storage (days)	120
Operating frequency (MHz)	49.9
Transmit elements (Yagi; 6dB forward gain)	4
Receive elements (phased array)	32
Transmitter Peak Power (kW)	0.1
Transmitter Average Power (W)	2
Transmit Time (s)	293.6
Pulse Repetition Interval (μs)	80
Pulse Length (μs)	1.667
Power consumption (kW @240V)	1
UHF Communication Link (MHz)	458

In the following manuscript, these surface current observations from VHF radar are described and used to characterize the coastal ocean environment at the SFOMC. Measurements from both moored and ship-board ADCPs are directly compared to these surface velocity measurements to establish the level of consistency between observing platforms. During quiescent atmospheric conditions, this approach provided data to examine the temporally evolving spatial current patterns at unprecedented resolution just inshore of the FC. Accordingly, the experimental design using the VHF radar is described in Section II. Prevailing coastal conditions are given in Section III. In Section IV, a detailed comparison is given between surface observations and moored and ship-based ADCP's from July 1999 experiment. Results are discussed in Section V with concluding remarks.

II. VHF RADAR MEASUREMENTS

An experiment was conducted in the summer of 1999 in the SFOMC. In this section, the VHF radar approach is described within the context of experimental design and spectral data quality of the observed surface current signals.

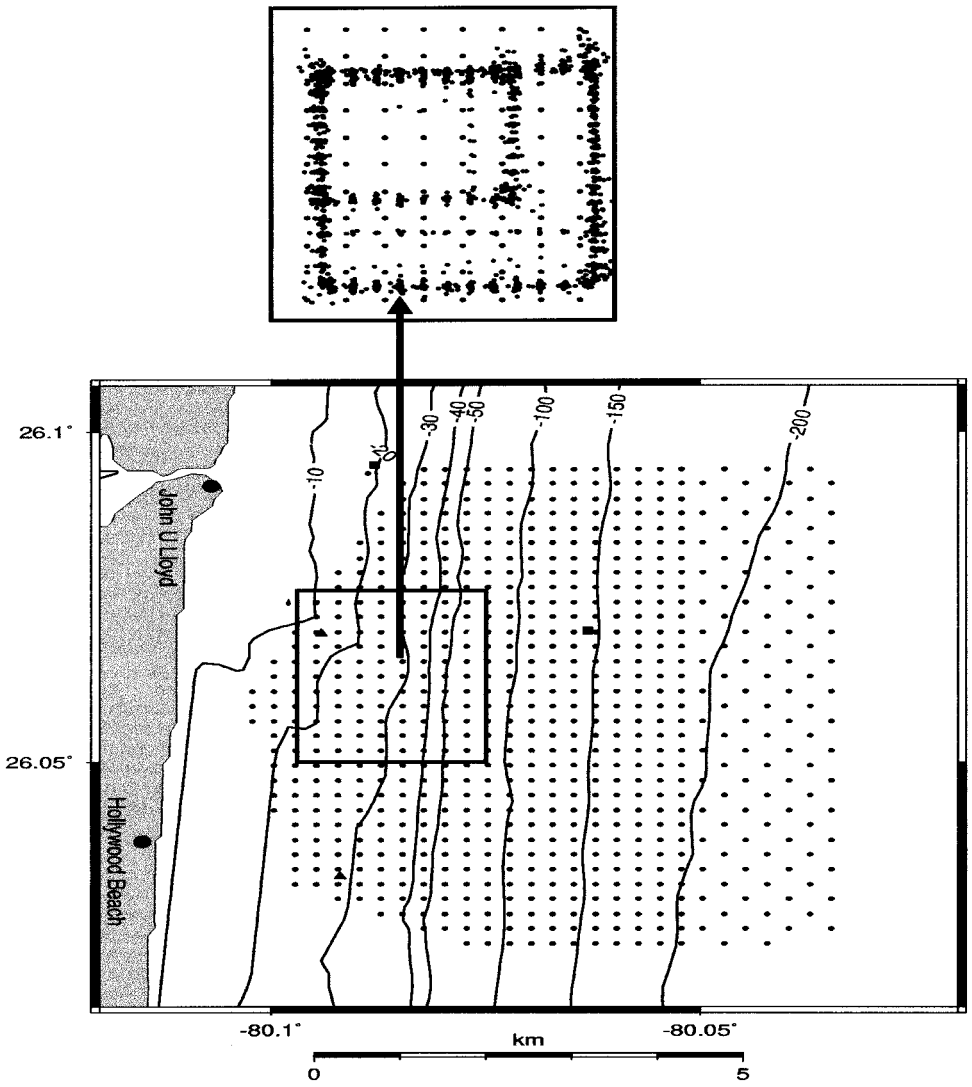

Fig. 1. VHF radar domain (circles) relative to USF/NOVA ADCP moorings (triangles: 50-m mooring at cell 244 is depicted as a red triangle), US navy ADCPs (boxes), and ship track (heavy black line). Inset provides the sampling positions of the ship from five cruises during the month-long experiment. Bottom topography is contoured at 10-m intervals to 50 m, then contoured at 50 m thereafter. Master and slave sites (heavy solid circles) were located at John U. Lloyd State Park and Hollywood Beach, respectively.

A. Experimental Design

The OSCR radar system was deployed in the SFOMC for a four-dimensional ocean current experiment starting on 25 June and ending 10 August 1999. During this period, a 29-d continuous time series of vector surface currents was acquired starting on 9 July and ending 7 August 1999 at 20-min intervals. The system consisted of two VHF radar transmit/receive stations operating at 49.945 MHz that sensed the electromagnetic signals scattered from surface gravity waves with wavelengths of 2.95 m. The VHF radar system mapped coastal ocean currents over a 7.5 km $\times$ 8 km domain with a horizontal resolution of 250 m at 700 grid points (Fig. 1). Radar sites were located in John U. Lloyd State Park (adjacent to the US Navy Surface Weapons Center Facility) (master: 26° $5.6'$N, 80° $6.4'$W) and an ocean-front site in Hollywood Beach, FL (slave: 26° $2'$N, 80° $6.7'$W), equating to a baseline distance of 6.7 km. Each site consisted of a four-element transmit and thirty-element receiving array (spaced 2.95 m apart) oriented at an angle of 37° (SW-NE at master) and 160° (SE-NW at slave).

Effective ranges of the HF and VHF modes of this pulsed radar differ significantly. As shown in Table I, the pulse repetition rates ($T_{\rm rep}$) is 80 μs and pulse duration for pulses ($T_{\rm dur}$) in VHF mode is 1.667 μs. Accordingly, the estimated effective range is

$$R = \frac{c}{2}\left(T_{\rm rep} - T_{\rm dur}\right) \tag{1}$$

where c is the speed of light (2.9998×10^8 m s^{-1}) [20]. For example, the VHF mode range is approximately 11 km while the effective range for the HF mode (25.4 MHz) is 44 km for the present OSCR configuration. These effective values are also important to the baseline separation distances. In the VHF mode, the baseline distances must be between 3–7 km to optimize the acquisition of the 2-D vector currents. By contrast, separation distances for an HF mode deployment are typically 20 to 35 km depending upon the configuration. In the 1994 Florida Keys experiment, for example, the baseline distance was about 38 km between two radar sites [12].

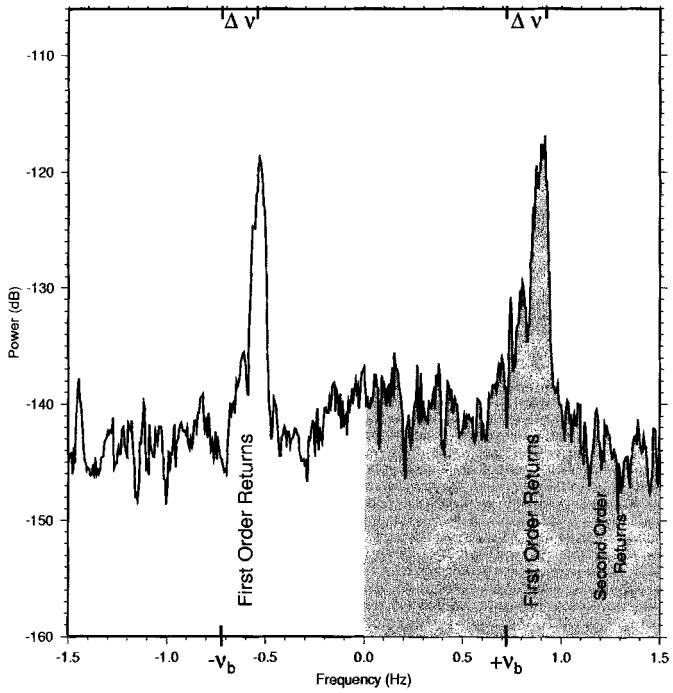

Fig. 2. Doppler spectrum from the 4-D current experiment at cell 300 showing the spectral peaks in power (dB) relative to the frequency (Hz). Bragg frequencies are depicted as $\pm\nu_b$ at 0.72 Hz as well as the frequency offset ($\Delta\nu$). The spectrum was smoothed using a nine point running average corresponding to 0.024 Hz. Frequency offsets of the spectral peaks for the advancing and receding wave field correspond to the radial current. Second-order returns contains information about the waves.

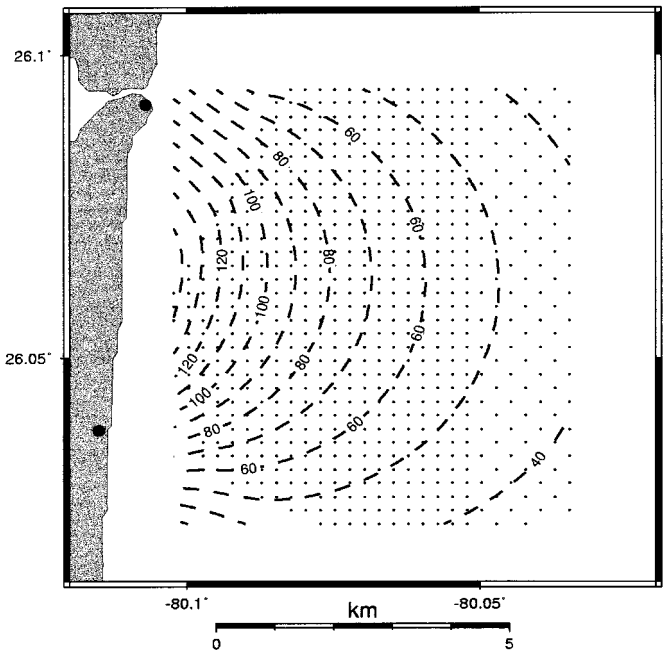

Fig. 3. Intersection angles (°) between the master and slave radial beams at each of the 700 OSCR cells. The contour interval is at 10° intervals labeled at 20° increments.

B. Bragg Backscatter

The corresponding Bragg frequency is

$$\nu_b = \sqrt{\left(\frac{g\nu_r}{\pi c}\right)} \tag{2}$$

where g is the acceleration of gravity (9.81 m·s^{-1}) and ν_r if the frequency of the radar (49.945 MHz). The resultant Bragg frequency is 0.721 Hz as shown in Fig. 2. Frequency offsets from the first-order Bragg peak ($\Delta\nu = \nu_o - \nu_b$) are proportional to the radial current for a wave advancing (positive) or receding (negative) from the radar station (i.e., $\Delta\nu = 2V_{cr}\lambda^{-1}$, where V_{cr} is the radial component of current along the direction of the radar). Given the range in the Doppler spectrum of $\pm$1.5 Hz, the maximum resolvable radial current is $\pm$4.4ms^{-1}. In the present context, the maximum current for the FC is expected to be 2 to 2.5 m·s^{-1}, well below this threshold in the Doppler spectrum. Notice that the first-order returns are above the noise floor of the Doppler spectra ($\approx$ 140 dB) for both advancing and receding waves. To obtain a 2-D vector current at the 700 cells, two transmit and receive stations are required to resolve the Doppler spectra as described elsewhere [20] and hence radial current measurements.

C. Radial and Vector Currents

Central to constructing reliable vector current fields from radial measurements is the intersection angle between the radials emanating from the master and slave stations (Fig. 3). Intersection angles crucially depend on the beach topography, which sets the geometrical constraints of the phased array. In this VHF domain, optimal intersections angles, defined here as $30° \leq \alpha \leq 150°$, encompassed nearly the entire domain except for the grid points closest to the shore and those just beyond the 40° limits in the northeast and southeast corners of the domain. These outer limits were at the maximum range of the master and slave radar stations of 11 km noted above. Thus, physical significance of the measurements in these areas will be avoided.

The Geometric Dilution Of Precision (GDOP) is used to quanitatively examine the spatial dependence of the observed current differences based on geometrical contraints. Using the radar's mean look direction (α) and the half-angle (ϕ) between intersecting beams [14], expressions for the error in the along-shelf (v) and cross-shelf (u) current components are

$$\sigma_v = \left\{2\frac{\sin^2(\alpha)\sin^2(\phi)+\cos^2(\alpha)\cos^2(\phi)}{\sin^2(2\phi)}\right\}^{1/2}\sigma \tag{3}$$

$$\sigma_u = \left\{2\frac{\cos^2(\alpha)\sin^2(\phi)+\sin^2(\alpha)\cos^2(\phi)}{\sin^2(2\phi)}\right\}^{1/2}\sigma \tag{4}$$

where σ represent rms current differences. The GDOP value is thus defined as the ratios of σ_v/σ and σ_u/σ for the along-shelf and cross-shelf currents, respectively. Over the VHF radar domain as shown in Fig. 4, the GDOP value ranged from 0.75 to 2. In the core of the domain where a large fraction of the subsurface measurements were acquired, the GDOP for both the along-shelf (v) and cross-shelf (u) currents was unity. Close to the coast, however, there was a large gradient in the GDOP increasing from 1 to 2 over a 1.5-2-km (6 to 8 cells) distance as intersection angles approached the limits (as suggested by Fig. 3).

An example of the two radial current plots (master and slave) and the corresponding vector current is shown in Fig. 5. The

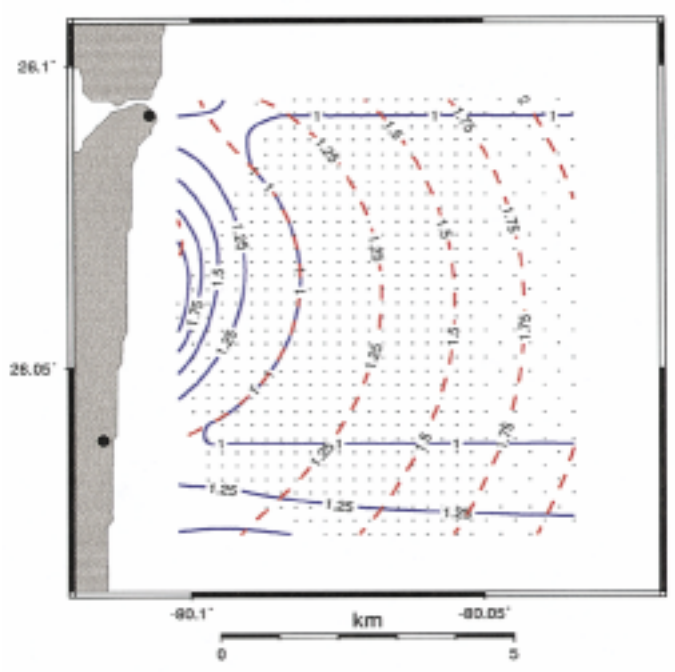

Fig. 4. GDOP for the along-shelf (red) and cross-shelf (blue) currents relative to the cells in the VHF radar domain.

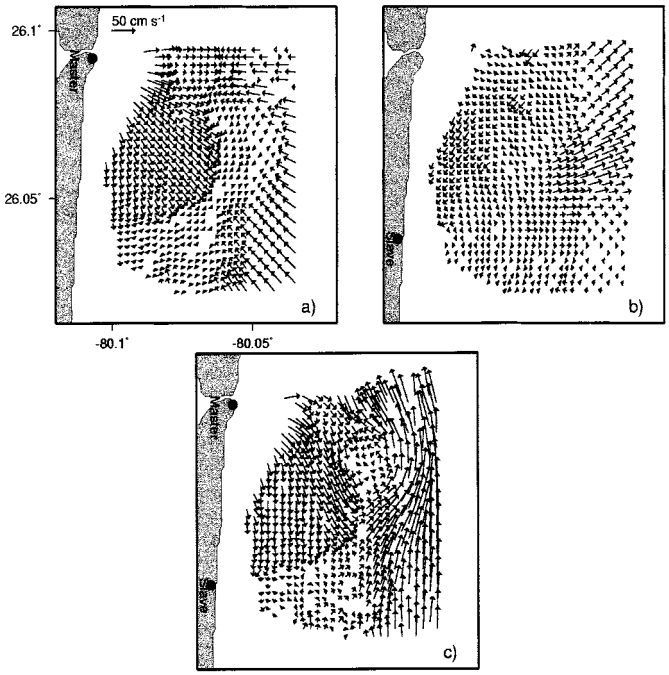

Fig. 5. Maps of a) master radial current, b) slave radial current, and c) vector current (cm s^{-1}) from 0400 GMT 26 June 1999. The scale of the current is given in a).

master radial current map indicated a current toward the southeast. On the periphery of this structure, radial currents were directed toward the radar site, indicating advancing peaks in the Doppler spectra. Radial currents from the slave station also indicated a southwest current in the same regime where master radial currents were toward the southeast [Fig. 5(b)]. In the central and southern portions of the VHF radar domain, the radial current field indicated flows in opposite directions with flows toward and away from the radar over the inner and outer parts of the radar domain, respectively. However, unless radial currents are in the same general directions of the prevailing current field, it is difficult to intrepret radial current patterns within the context of physical processes. It is more appropriate to convert radial currents to a 2-D current vector consisting of two cartesian current components.

As each OSCR cell (250 m $\times$ 250 m) has its own unique bearing and distance from each site (i.e., Fig. 3), the cross-shelf current at any given cell is

$$u = \frac{r_m \cos(\theta_s) - r_s \cos(\theta_m)}{\sin(\theta_s - \theta_m)} \tag{5}$$

and the along-shelf current is

$$v = \frac{r_s \sin(\theta_m) - r_m \sin(\theta_s)}{\sin(\theta_s - \theta_m)} \tag{6}$$

where $r_{m,s}$ represent radial currents and $\theta_{m,s}$ represent bearing angles relative to the boresites from the master(m) and slave(s) stations, respectively [21]. As shown in Fig. 5(c), the vector current field ($w = u + iv$) is constructed from (5) and (6) based on observed radial currents (5a,b) and bearing angles. For this particular snapshot, these data indicated a submesoscale vortex (radius of 1.25 km) rotating cyclonically. Offshore of the vortex was the inshore edge of the FC where surface currents exceeded 50 cm·s^{-1}. Inshore of the vortex, a predominant southward current of 20 to 30 cm·s^{-1} was observed, suggesting fairly complicated physical processes over the inner to middle shelf.

D. Spectral Data Quality and Return

Over the course of the experiment, a total of 2078 samples was acquired from 0320 GMT 9 July (YearDay 191) until 2340 GMT 6 August (YD 220) yielding a 29-d time series. Of the 2078 samples, only 69 samples were missing from the vector time series, equating to a 3.3% loss of the 20 minute snapshots. Previous HF radar experiments have typically yielded data returns of 93% to 97% [7], [11], [12]. Thus, these experimental results using the VHF mode were on the higher end of the limits with respect to overall data return relative to previous experimental results.

As shown in [22], the spectral quality index takes into consideration: the size of the largest peak (in decibels); the number of Bragg peaks in the spectrum (either 2,1,0); the Bragg ratio (difference between positive Bragg peak and negative Bragg peak in decibels where the smaller the Bragg ratio, the higher the quality number); the width of the largest Bragg peak (the top quality numbers (7,8,9) require that least one Bragg peak spans 0.022 Hz in frequency space); and the error in the Bragg peak separation. This index is an integer in the range of 0 to 9, where 9 being the highest quality index. During the course of this experiment, this spectral quality index from both the master and slave radar stations ranged between 3 to 7 (Fig. 6). Notice that higher spectral quality from each site was closest to the coast as signal strength of ground wave signals is a function of both transmit frequency and sea water conductivity. As frequency increases, transmitted signals attenuate quicker than those of lower frequencies [3]. Of equal importance, the conductivity of

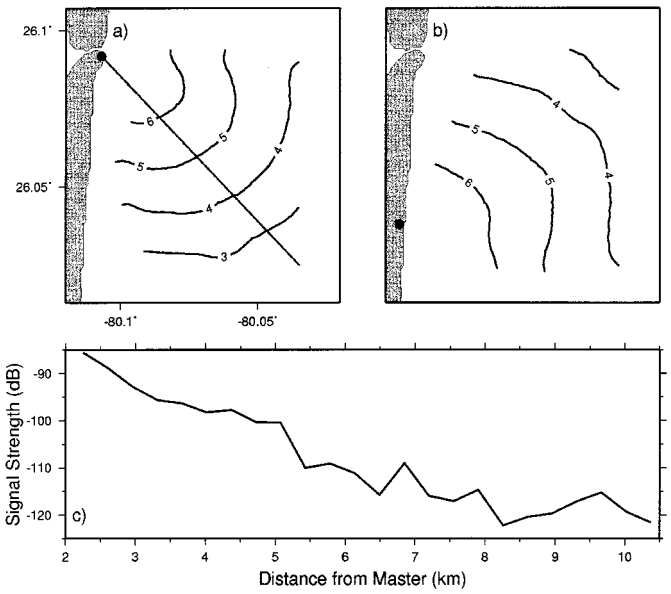

Fig. 6. Spectral quality numbers from a) master and b) slave stations based upon the spectral data in the Doppler spectra and c) the signal strength (dB) along a radial emanating from the master site (solid line in panel a). High spectral data quality number corresponds to good separation between the first-order peaks and the noise floor and well-defined Bragg ratios. Notice that in the far-field relative to the master and slave stations (10–11 km) the spectral quality numbers and signal strength decrease to 3 and −120 dB.

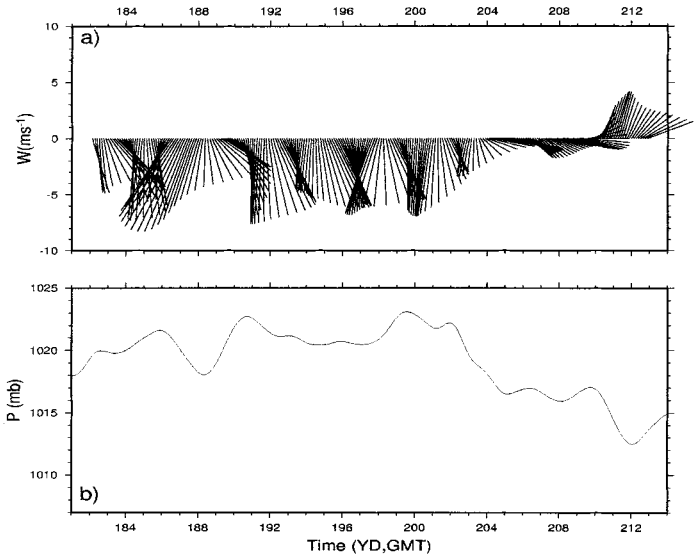

Fig. 7. Forty-hour low-pass filtered a) surface wind (m s^{-1}) and b) surface pressure (mb) from hourly observations at the CMAN station at Fowey Rocks located south of the VHF radar domain in July–August 1999. Surface wind was placed into an oceanographic context and then rotated 90° cyclonically. A positive value for the wind represents offshore flows whereas a negative value represents onshore surface winds.

the sea surface plays an important role in ground wave propagation. As conductivity increases, signal attenuation decreases exponentially with distance offshore. This is precisely why HF radar techniques attenuate by 40 dB after just a few kilometers over fresh water. Based on CTD measurements from the moorings and the *R/V Stephan* [23], the corresponding conductivities exceeded 5.5 $\mho \cdot \mathrm{m}^{-1}$, providing a good conducting plane for ground wave propagation. Even in the far-field, typically 10 km from the radar sites, spectral data quality decreased only to 3, which was sufficient to resolve the currents. Along one of the radial legs, the signal-to-noise ratio (SNR), defined as the difference between the strength of the Bragg peak and the noise floor, decreased by about 30 dB from the coast to the far-field [see Fig. 6(c)]. As spectral quality indicies decrease toward unity, current signals cannot be resolved from the Bragg peaks in the spectra and are eliminated from further analysis. Here, as the spectral quality index remained at 3 or above, radar-derived currents were of sufficient quality to warrant a detailed comparison to subsurface current observations from the mooring and ship-based measurements.

III. Observations

A. Atmospheric Conditions

Prevailing atmospheric conditions during the experiment were relatively calm as indicated by near-surface wind and pressure records from a Coastal Marine Automated Network (CMAN) station at Fowey Rocks (25°35.4′N, 80°6.′W), which was located approximately 70 km south of the domain. As shown in Fig. 7, 40-h low-pass filtered surface winds were onshore ranging between 3 to 7 m·s^{-1}. On YD 202, surface winds reversed to a southerly then to an offshore wind as the pressure decreased from 1023 to 1012 mb over a 10-d period [Fig. 7(b)]. During this weak pressure change, surface winds were 4 to 6 m·s^{-1}. Averaged over the month time series, the mean wind speed was 4.5 m·s^{-1} directed toward 210°T. Meteorological conditions at the Lake Worth CMAN station (26°37′N, 80°03′W, not shown) were similar to these observations from Fowey Rocks. Based upon these data, the mean wind-induced surface current was estimated to be 6 cm s^{-1} for an Ekman depth of 30 m. Theoretically, the steady-state, wind-induced surface flows should be directed 45° to the right the wind; however, in this case, the mean coastal currents were directed toward the north opposing the mean wind direction.

Surface wave measurements at the NOVA/USF mooring in 11 m of water revealed significant wave heights of 1 m or less during the first half of July where the surface gravity waves had periods between 4–6 s. Based on the deep-water dispersion relation, these waves had horizontal wavelengths of about 40 m for a 5-s wave. The estimated Stokes drift at the surface was 5–6 cm·s^{-1} for a mean wind speed of 4.5 m·s^{-1}[21]. Given a vertical dependence of e^{-2kz} where k is the wavenumber of the dominant wave ($\approx \pi/20$ m), the estimated current difference for this Stokes wave component was less than 1 cm·$s^{-1} \cdot \mathrm{m}^{-1}$ between the surface and 4-m depth. Thus, during the observational period, surface winds and waves did not appear to significantly impact the surface velocity field compared to oceanic forcing induced by the FC intrusions across the shelf break.

B. Surface Current Observations

An example of the observed surface current variability is shown in Fig. 8 over a 3-d period, including FC intrusions. On 18 July (YD 200), surface velocities exceeded 1.4 m·s^{-1} between 5 to 7 km offshore with a large surface current gradient near the shelf break. Closer to the coast, surface currents were weaker with velocities of 20 to 30 cm·s^{-1}. Over the next 8

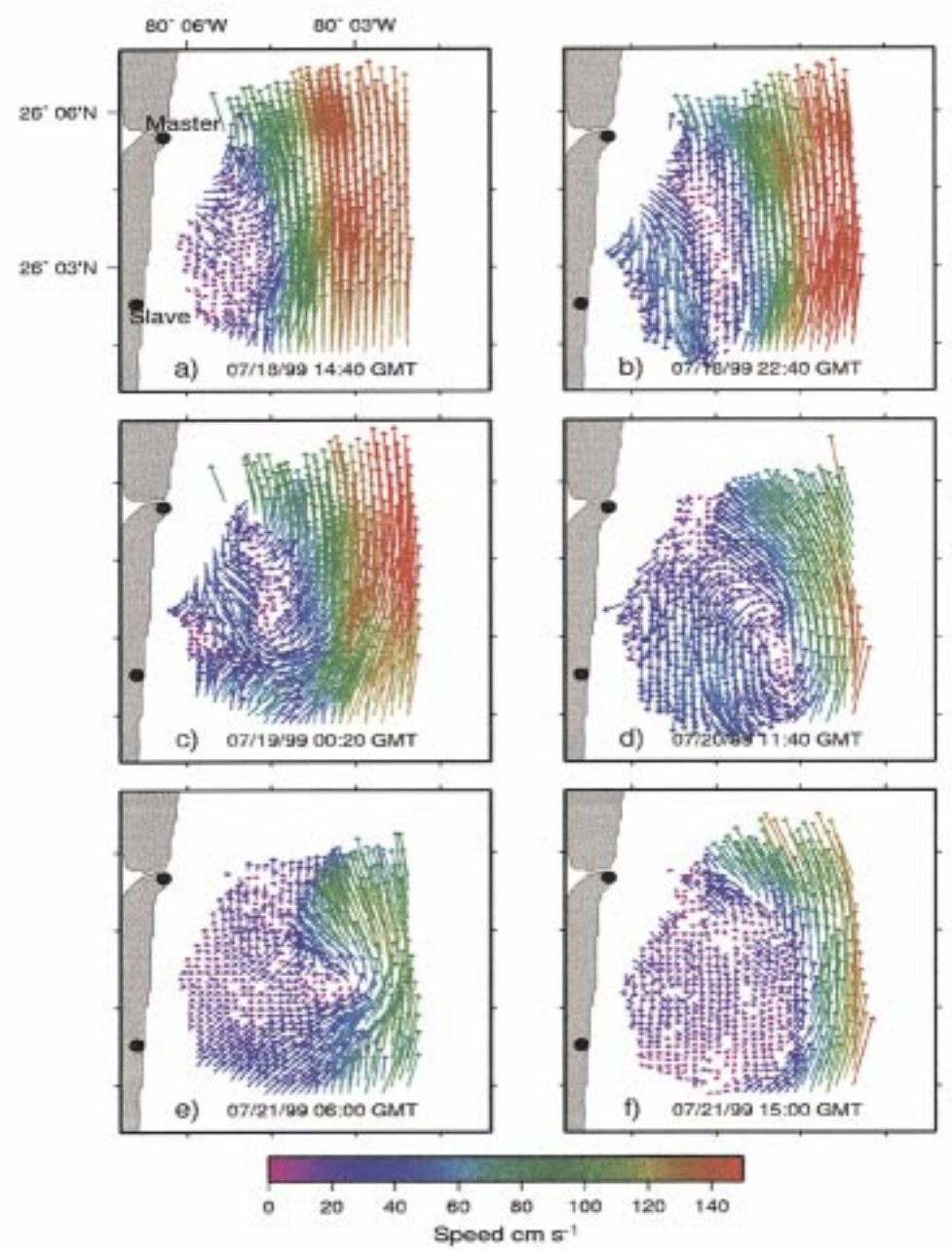

Fig. 8. Surface current imagery from 18–21 July 2000 during the SFOMC 4-D current experiment off Ft. Lauderdale for: (a) 1440 GMT 18 July, (b) 2240 18 July, (c) 0020 GMT 19 July, (d) 1140 GMT 20 July, (e) 0600 GMT 21 July, and (f) 1500 GMT 21 July. The color of the current vectors depicts magnitude of the current as per the color bar.

h [see Fig. 8(b)], coastal currents flowed south at about 60 cm·s^{-1} and a region of weak currents was observed along the shelf break. Surface velocities also indicated along-shelf curvature in this surface current gradient regime. Two hours later [Fig. 8(c)], surface velocities rotated cyclonically along the shelf break where a surface current convergence developed in the southern part of the domain. Surface velocities greater than 1 m·s^{-1} were located approximately 5 to 7 km offshore during an intrusion by the FC. Approximately 11 h later, a cyclonic vortex was observed with a radius of 1.5 km. During this time, near-shore currents were 40 to 50 cm·s^{-1} whereas offshore currents ranged between 80 to 90 cm·s^{-1} in the FC. This velocity difference was associated with an asymmetric vortex, but with larger currents and radii than that observed on 26 June [18]. At 0600 GMT 21 July (YD 203), surface currents indicated cyclonic curvature about 5 km offshore with a weak surface convergence zone in the domain's center. Coastal currents at this time were weaker (20 cm·s^{-1}) compared to currents of 70 cm s^{-1} along the inshore edge of the FC. Subsequently, surface currents indicated a larger-scale vortex with weaker currents or perhaps a frontal lobe-like structure 9 h later [Fig. 8(f)]. These images over a 3-d time period exemplified a dynamic coastal regime with FC intrusions, lobe-like structures and multiple-scale vortices. In fact, these energetic vorticity regimes scaled as 3 to 4f (where f is the local Coriolis parameter) due primarily to gradients in the cross-shelf direction ($\partial v/\partial x \gg \partial u/\partial y$) [19]. Similar surface current variability was also found in the vorticity fields along

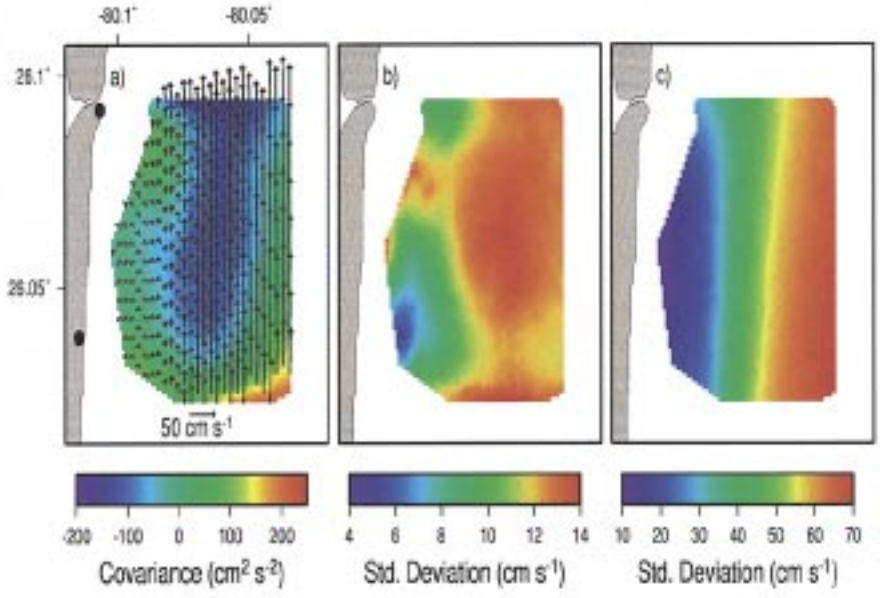

Fig. 9. a) Time-averaged mean current (arrows) superposed on covariance of the observed surface flows and standard deviations of b) cross-shelf and c) along-shelf surface currents estimated from the 29-day mean current in a). Color bar depicts the covariance estimates ($cm^2 \cdot s^{-2}$) and standard deviations ($cm \cdot s^{-1}$). Notice that the along-shelf standard deviation (panel c) is 2 to 5 times larger than in the cross-shelf direction (panel b).

the Florida Keys during an HF radar experiment in May 1994 [12].

To further illustrate this spatial surface current variability, the time-averaged mean, covariance, and standard deviations were estimated from the 29-d time series (Fig. 9). Time-averaged mean flows were aligned in the along-shelf direction and opposed the mean surface winds as noted above. Beyond the shelf break, northward currents exceeded 50 $cm \cdot s^{-1}$, consistent with the close proximity of the FC to the coast. Inside the shelf break, mean flows were considerably weaker with currents of 10 to 20 $cm \cdot s^{-1}$, generally directed toward the north. In the central portion of the mapped domain, the covariance between the cross-shelf and along-shelf flows revealed an elongated regime where covariance estimates were less than $-100\ cm^2 \cdot s^{-2}$ due in part to the observed cyclonically rotating vortices and lobe-like structures (i.e., Fig. 8). The covariance between the cross-shelf and along-shelf currents was positive surrounding this covariance minima where values exceeded 100 $cm^2 \cdot s^2$ along the eastern edge of the vortex region. Standard deviations for the cross-shelf [Fig. 9(b)] and the along-shelf [Fig. 9(c)] currents differed by a factor of 2 to 5 depending on their location. For example, along the inner and outer edge of this covariance minima, cross-shelf standard deviations were a maximum of 12 to 14 $cm \cdot s^{-1}$ compared to 40 and 70 $cm \cdot s^{-1}$ in the along-shelf current's standard deviation. These time-averaged estimates of the surface current statistical properties suggests substantial cross-shelf variability in the along-shelf surface current structure, particularly in the vortex-dominated regime. One possibility is that this regime was dominated by wave-like features [19].

C. Ship-Based Measurements

Ship-based ADCP measurements of horizontal current profiles with an RDI 5-beam, 600-kHz broad-band ADCP and of the stratification with an Ocean Sensors (OS500) CTD were acquired from the *R/V Stephan* during AUV operations. The ADCP was deployed over the starboard side of the *R/V Stephan*. Shipborne CTD and ADCP measurements were acquired over a rectangular box pattern (see Fig. 1). The eastern, north–south leg of the ship track was positioned beyond the shelf break (coincident with the *third reef*) because high horizontal and vertical shear tended to occur beyond or just east of the shelf break. The typical ship speed along the transects was 1.5 $m \cdot s^{-1}$ such that the ship track boxes required 1.5 to 3 h to complete.

As shown in Fig. 10, the ADCP was set to 1-m bins, producing a vertical range of about 35 m depth. Bottom tracking was possible at depths up to 85 m. Note that all observations (15-s ensemble averages) had valid bottom tracking and differential GPS (DGPS) navigation data were logged along with the ADCP output. Two cross-shelf sections of the along-shelf flow indicated the extreme oceanic conditions that frequently occurred in this regime. Relatively weak southward flow was observed over the shelf and shelf break at 0400 GMT 16 July with weak vertical current shear of $10^{-2}\ s^{-1}$. Fifteen hours later (1900 GMT), the FC intruded over the shelf as upper ocean currents increased to 80 $cm \cdot s^{-1}$ [upper right edge of Fig. 10b)] although there was still southward flow of 20 $cm \cdot s^{-1}$ over the inner-shelf [Fig. 10(b)]. With the FC so close to the shelf, strong vertical shears were also evident in the ADCP measurements. Such flow reversals occurred both on relatively long-time scales of days and relatively short-time scales of 3, 10, and 27 h. These ship-board measurements revealed complicated and highly intermittent FC forcing events across the shelf break that affected the coastal circulation.

D. Moored Measurements

The University of South Florida (USF) and NOVA Southeastern University deployed three moored ADCP arrays in the SFOMC as shown in Fig. 1. These profilers sampled the current

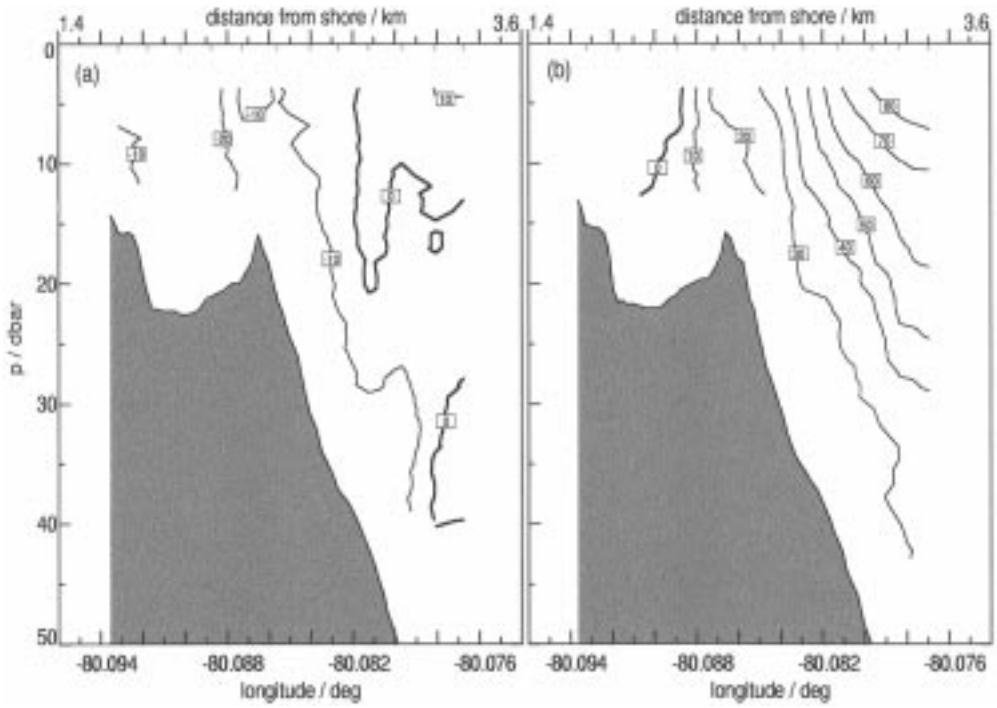

Fig. 10. Cross-shelf sections of the along-shelf currents from the shipboard 600 kHz ADCP on the *R/V Stephan*: (a) 16 July 1999, 0403 GMT and (b) 16 July 1999, 1849 GMT. The latitude of the data is 26.053°N. Velocity is contoured at 10 cm·s^{-1} intervals. The zero velocity contour is a heavy, dark line.

structure at 15-min intervals from an upward-looking 300-kHz ADCP at the 11-m mooring and two downward-looking 600-kHz ADCPs at 20- and 50-m depths. The bin size at the 11- and 20-m moorings was set to 0.5 m while a bin size of 1 m was used at the 50-m mooring. In addition, microcats were deployed at both the NE and SW moorings to measure temperature, conductivity, salinity, and density fields at 5-min intervals at several vertical levels. Data acquisition started on 25 June at the 11-m mooring and on 15 July (YD 197) at the NE and SW mooring sites. For the purposes of this manuscript, the 50-m mooring ADCP measurements acquired near the center of the radar domain will be used in the comparisons below where the GDOP was unity in both current directions (see Fig. 4).

As shown in Fig. 11, coherent structure was observed throughout the water column in July and early August where the current ranged from −50 to 100 cm·s^{-1}. Initially, a near-daily oscillatory current of 20 to 30 cm·s^{-1} was observed with larger currents near the surface. Near YD 201, currents throughout the column indicated an along-shelf flow of 30 cm·s^{-1} toward the south. The current structure then reversed to a predominate, northward along-shelf current until about YD 206 when the current became oscillatory with amplitudes exceeding 50 cm·s^{-1}. Subsequently, an FC intrusion was observed between YD 210 to 213 over the 50-m isobath. The current during this time was in the along-shelf direction with weak cross-shelf flows. Upper ocean currents approached 100 cm·s^{-1}, that decreased to about 40 cm·s^{-1} near the bottom. Strong oscillatory currents were also evident after this FC intrusion. Over the 23 days of coincident measurements, the currents seemed to be *predominantly* barotropic with relatively weak cross-shelf flows.

RMS differences between adjacent ADCP bins were examined from 3 to 40 m (not shown) to understand subsurface current variability. For the cross-shelf current, bin-to-bin variability was 2 to 3 cm·s^{-1} in the upper 10 m, decreasing to 2 cm·s^{-1} at depth. By contrast, bin-to-bin variability was 5 to 7 cm·s^{-1} in the upper 10 m for the along-shelf current, decreasing to 3 cm·s^{-1} below 10 m. As suggested by ship-board measurements, this variability is relevant to the comparisons to the surface currents discussed below.

IV. Comparisons

Observations described in Section III indicated sufficient veracity to warrant a comparison between the radar-derived surface signals and subsurface measurements from the ADCP on the mooring (fixed frame) and the *R/V Stephan* (moving frame). To place these comparisons into context of other radar derived data sets, published analysis techniques will be used to examine the differences. The difference here is that the spatial resolution of the surface current is now 250 m vice 1.2 km, yielding a significantly higher resolution surface velocity field that resolved submesoscale processes. One statistical measure of the correlation between two differing measurements is the complex correlation coefficient

$$\gamma = \frac{\langle u_o u_b + v_o v_b \rangle + i \langle u_o v_b - v_o u_b \rangle}{\langle u_o^2 + v_o^2 \rangle^{1/2} \langle u_b^2 + v_b^2 \rangle^{1/2}} \tag{7}$$

and the complex phase angle

$$\phi = \tan^{-1} \frac{\langle u_o v_b - v_o u_b \rangle}{\langle u_o u_b + v_o v_b \rangle} \tag{8}$$

where $\langle \ldots \rangle$ represents an average (based upon n points) [23] for the surface ($_o$) and subsurface ($_b$) currents. This phase angle represents the average cyclonic angle of the subsurface current vector with respect to the surface current vector.

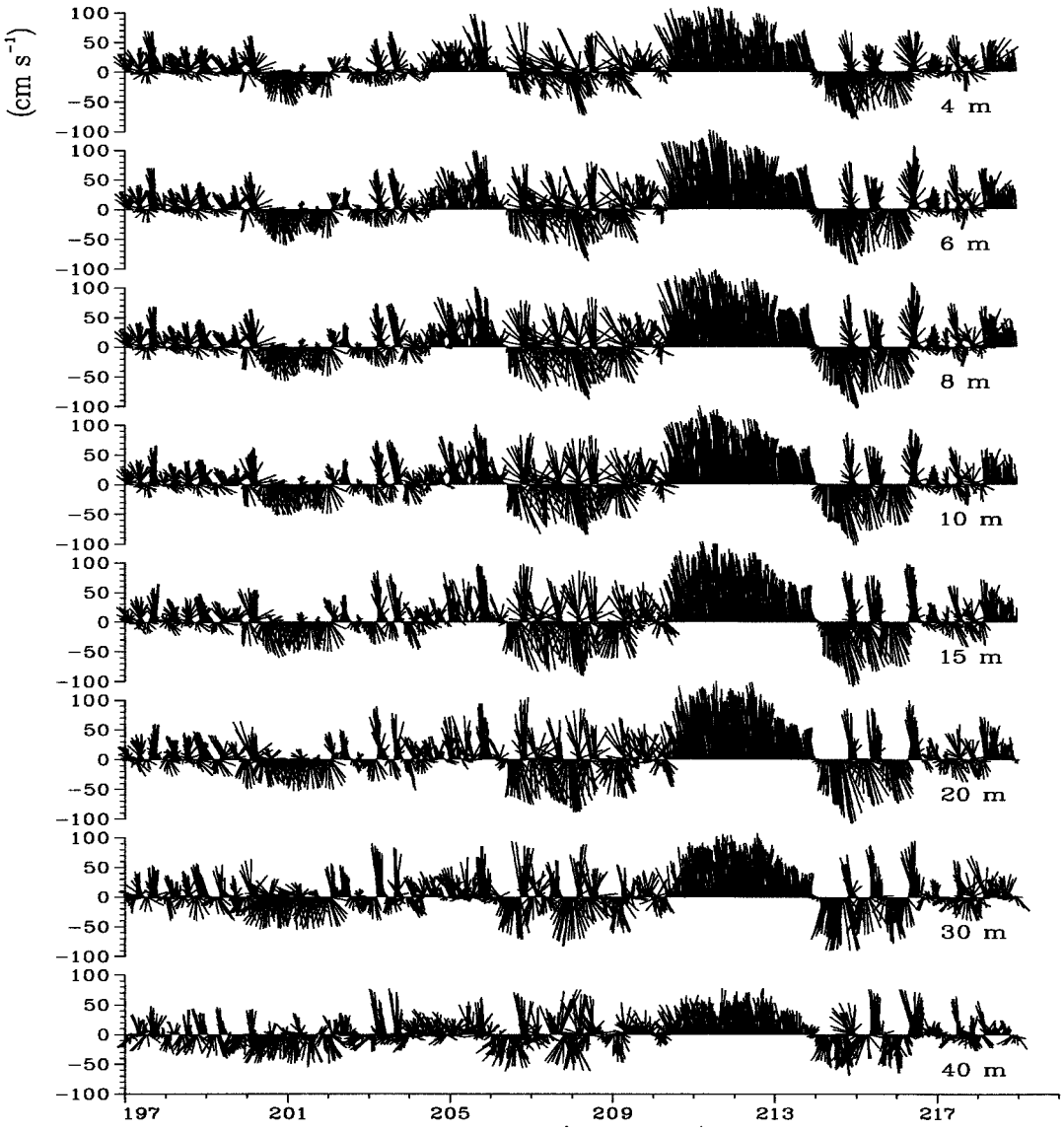

Fig. 11. Vector plot of the time series at the USF/NOVA 50-m mooring at selected depths through the column starting on 15 July and ending on 8 August 1999. A northward current (°T) is a vector pointing upward toward the top of the page.

A. Fixed Frame

To facilitate direct comparisons between the surface and subsurface velocities, the current profiler data from the downward-looking ADCP were smoothed using a 3-point Hanning window and subsampled at 20-min intervals, yielding 23 d of coincident measurements. As shown in Fig. 12, surface currents in the upper 0.2 m are compared to subsurface currents at 3.2 m from the 50-m mooring. Since the currents from the 3.2- and 4.2-m bins indicated similar fluctuations, we chose the 3.2-m bins for the time series comparisons. In the along-shelf direction (v), subsurface currents were at times larger than surface currents particularly when the FC moved toward the coast. Notice that the cross-shelf currents (u) were weaker than those in the along-shelf direction by at least a factor of two. Over this 23-d time series, surface and subsurface currents were correlated at levels exceeding 0.8. From YD 208 to 209, complex phases were -16°, suggestive of an anticyclonic or clockwise veering of subsurface currents relative to the surface values. Moreover, the corresponding density time series (not shown) acquired at the 50 m mooring location indicated isopycnal displacements of 5 to 10 m during this period. This significant baroclinicity explains a fraction of the observed differences between a fresher surface layer and more dense subsurface layers where the bulk current shear between 0.2 m (surface) and 3.2 m depth ranged from 0.2 to 5×10^{-1} s^{-1}. These levels of bulk current shears have been documented in other coastal regimes directly influenced by the Gulf Stream [7] and the FC [12] as more dense, subtropical water may have been subducted underneath the fresher, coastal waters as observed off Cape Hatteras [24].

Multilevel current data from 3.2 and 4.2 m beneath the surface were then regressed to the surface current (Fig. 13). At the 3.2-m level, the scatter for the cross-shelf current revealed a slope of 1.37 between the subsurface and surface currents [Fig. 13(a)] with a bias of 4.8 cm·s^{-1}. The peak in the current differences was located at zero difference and these differences were normally distributed. As the along-shelf current was more energetic

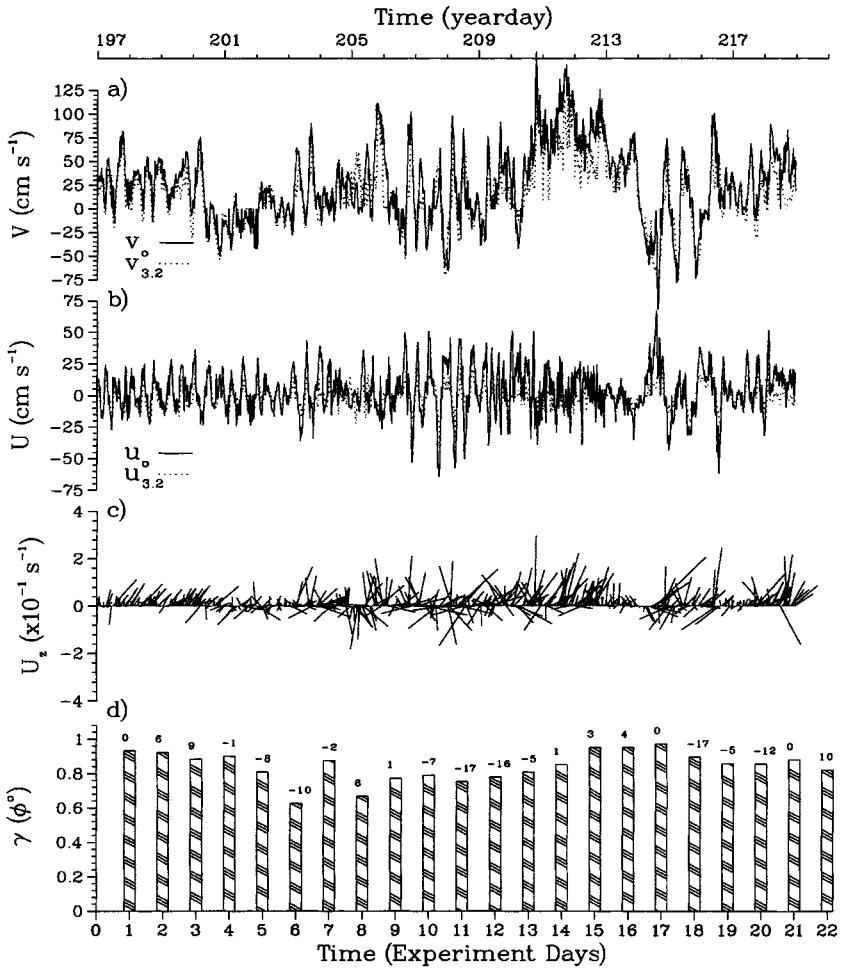

Fig. 12. Comparison of OSCR-derived surface and subsurface (3.2 m) current time series from a downward-looking ADCP attached to a surface mooring along the 50 m isobath deployed by USF/NOVA for: (a) along-shelf component (cm s^{-1}), (b) cross-shelf component (cm·s^{-1}), (c) bulk current vector shear ($\times 10^{-1}$ s^{-1}) defined as the current differences within panels a and b divided by a depth difference of 3 m and (d) daily complex correlation coefficients (γ) and phase angles ($\phi(^\circ)$: located at the top of the bars) relative to the surface velocity. A negative phase implies an anticyclonic current veering with depth.

than the cross-shelf current, the bias was 8.9 cm·s^{-1} with a slope of unity [Fig. 13(b)]. The frequency distribution in this case suggested a slight positive shift of 5 cm·s^{-1} in the current differences. Similar results were also apparent in the comparisons at 4.2 m where the cross-shelf current bias was 3.8 cm·s^{-1} with a slope of 1.31 [Fig. 13(c)]. By contrast, along-shelf current differences indicated a bias of 8.4 cm·s^{-1} again with a slope of 1 [Fig. 13(d)]. These results suggest that the measurements in the upper few meters of the water column at the 50-m mooring were quanitatively consistent with surface currents.

Surface velocities at the 50-m mooring (i.e., cell 244 depicted as a red triangle in Fig. 1) were used to estimate the complex correlation and phase as per (7) and (8) averaged over the 29-d time series at each of the radar cells. As shown in Fig. 14, correlation coefficients were elongated in the along-shelf direction with a maximum of 1 at the 50 m mooring. Notice the marked spatial change in the correlation coefficient in the cross-shelf direction. Correlation indices decreased by 0.2 km^{-1} in the onshore direction, whereas in the offshore direction, the correlation coefficient decreased by only 0.1 km^{-1}. Given the presence of the FC and its influence on the coastal ocean, the larger correlation gradient was in the onshore direction. Complex phase angles ranged from -25° in the southwestern portion of the domain compared to 10° in the northwestern part of the domain. The phase angles revealed an anticyclonic veering of

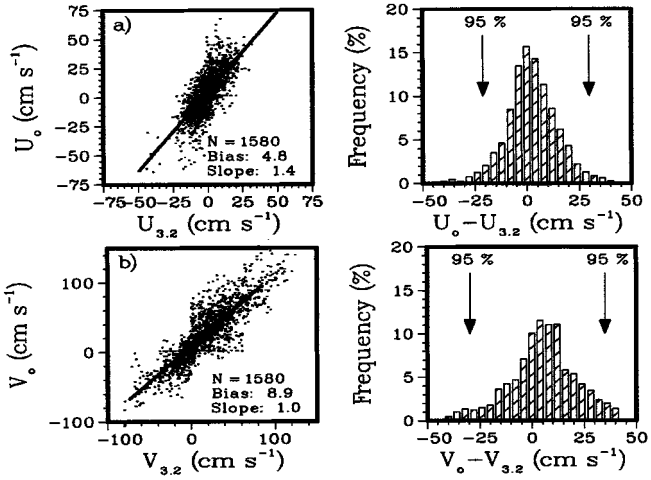

Fig. 13. Scatter diagrams (left) histograms (right) for the comparisons of surface and subsurface currents at the 50-m mooring at 3.2 m (panels a,b) and 4.2 m (panels c,d).

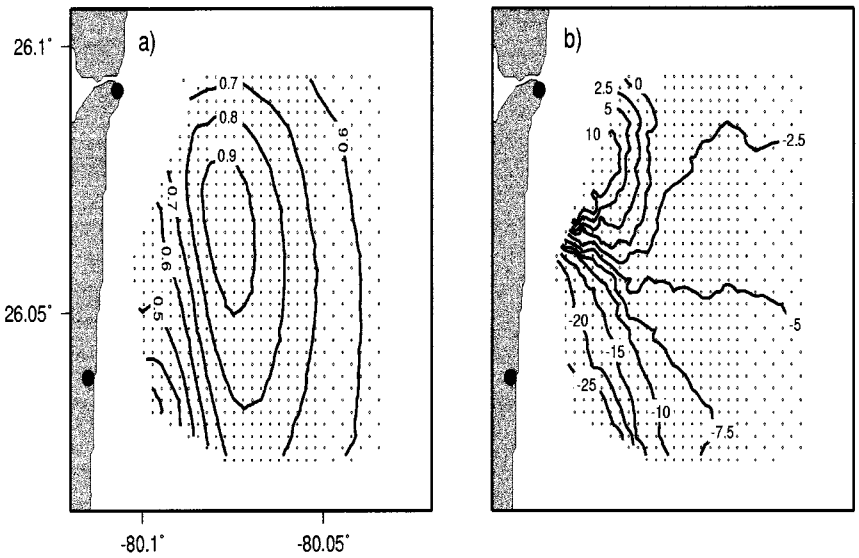

Fig. 14. a) Complex correlation and b) phase (°) relative to the OSCR cell 244 (red tirangle in Fig. 1) corresponding to the 50 m USF mooring for the 29-d time series. The correlation coefficient is contoured at 0.1 intervals and the complex phase is contoured at 2.5° increments.

TABLE II
AVERAGED DIFFERENCE BETWEEN THE SURFACE AND SUBSURFACE CURRENTS (3 M, 4 M, AND DEPTH-AVERAGED) FOR SPEED (V_{o-b}), DIRECTION (θ_{o-b}), EAST–WEST (u_{o-b}) COMPONENT, NORTH–SOUTH (v_{o-b}) COMPONENT, COMPLEX CORRELATION COEFFICIENT (γ), PHASE (ϕ) AND THE RMS DIFFERENCES IN THE EAST–WEST ($u_{o-b_{\rm rms}}$) AND NORTH–SOUTH ($v_{o-b_{\rm rms}}$) VELOCITY COMPONENTS BASED ON MOORING AND SHIP TRANSECT DATA DURING THE JULY 1999 EXPERIMENT AT SFOMC

Series	V_{o-b} cm s^{-1}	θ_{o-b} (°)	u_{o-b} cm s^{-1}	v_{o-b} cm s^{-1}	γ	ϕ (°)	$u_{o-b_{rms}}$ cm s^{-1}	$v_{o-b_{rms}}$ cm s^{-1}
Mooring								
$\vec{V}_{3m}$	11.7	-14.7	4.3	9.6	0.87	-1.2	13.7	22.2
$\vec{V}_{4m}$	8.7	-13.3	3.7	8.5	0.88	-1.8	13.2	20.5
$\vec{V}_{da}$	7.7	-20.3	4.1	11.7	0.83	-2.0	14.8	22.8
Ship								
$\vec{V}_{3m}$	4.1	7.0	-9.7	-0.2	0.87	-17.0	17.5	14.
$\vec{V}_{da}$	2.1	-0.8	-9.7	6.4	0.82	-18.9	17.4	14.8

the current vector except in the northwest quadrant where the phase angle veered in the cyclonic direction relative to the surface velocity at 50 m. While the mooring comparisons showed reasonably good correlation indices, the surface velocity structure was highly variable and required cross-shelf measurements from ship, mooring or AUV platforms to resolve submesoscale current structure [18], [19].

Averaged current differences from 23 d of coincident measurements are listed in Table II. In terms of current speeds, there was a 11.7-cm·s^{-1} difference between the surface and 3.2-m value. This difference decreased to about 8.7 cm·s^{-1} at 4.2-m depth. The difference between the depth-averaged and the surface currents was slightly less, suggesting the relative importance of the depth-averaged flows [19]. Similarly, the differences in the current direction were 13 to 14° at both 3 and 4 m beneath the surface. Regardless of the 3.2-m, 4.2-m, or depth-averaged comparisons to the surface flow, correlation coefficients exceeded 0.8 with complex phases of -1 to $-2°$. Of particular importance here, rms differences ranged between 13 to 22 cm·s^{-1} for the velocity components. Given the bin-to-bin current variability in the ADCP measurements of 3 to 7 cm·s^{-1} in the upper 10 m, these rms differences actually ranged between 10 to 15 cm s^{-1}, consistent with previous findings. Moreover, these rms current differences may not necessarily represent just measurement error. Measurement error for the radar-derived currents has been cited to be between 4–5 cm·s^{-1} while measurement error for ADCP-derived currents is 1 to 2 cm·s^{-1}. Thus, a large fraction of these differences may be associated with the geophysical variability as observed in previous sets of radar-derived surface current measurements. These VHF radar-derived surface velocities were reliable and reflective of a highly energetic coastal regime influenced by the FC at the SFOMC.

B. Moving Frame

Downward-looking ADCP profiles and CTD measurements from the *R/V Stephan* were also acquired during the experiment from several days of measurements. Of particular interest is to examine the 3-m bin data and the depth-averaged flows in terms of correlating the signals to the radar-derived signals. The closest radar measurement in time and space to each ship profile was used in these comparisons following [14]. As shown in Fig. 15, comparisons at the 3-m bin revealed similar regression slopes in both the cross-shelf and along-shelf directions. In the cross-shelf direction, for example, the slope was about 1.4 with a bias of -8.1 cm s^{-1}. However, the scatter was much greater than that observed at the mooring site as reflected by the 10 cm·s^{-1} current differences in the histograms. The scatter in the along-shelf current direction was also much less and more consistent with mooring results. For these data, the slope approached unity with a bias of 4.3 cm·s^{-1}. In both cases, current differences were normally distributed falling within a 95% confidence band as in the mooring data.

Given the relatively shallow depths along the ship transects, the ADCP current profiles were vertically averaged and compared to the surface current as shown in Fig. 16. There was less scatter ($\pm$20 cm·s^{-1}) in the cross-shelf direction than in the 3-m comparison and the slope of the regression curve was 1.18 with

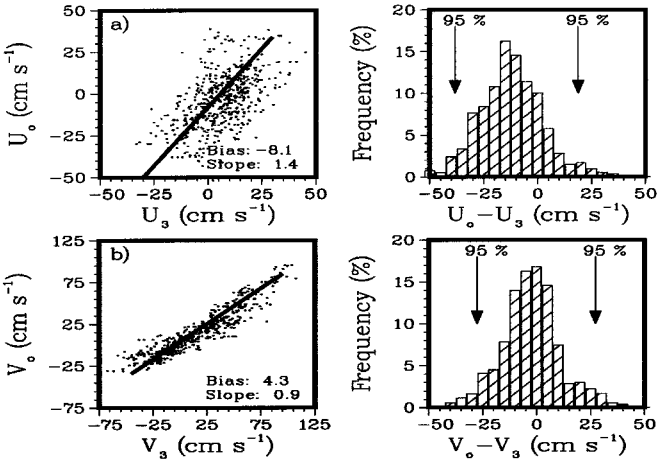

Fig. 15. Scatter diagrams (left panel) histograms (right panel) for the comparisons of a) cross-shelf and b) along-shelf surface ($_o$) and the 3-m subsurface currents ($_3$) from the ship transects in the VHF radar domain.

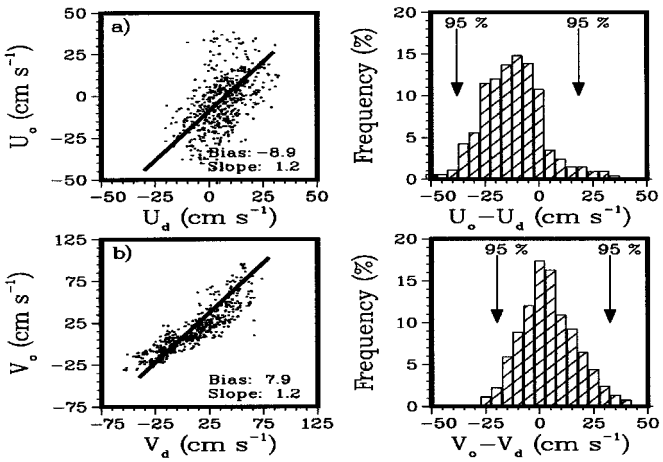

Fig. 16. Scatter diagrams (left panel) histograms (right panel) for the comparisons of a) cross-shelf and b) along-shelf surface ($_o$) and the depth-averaged subsurface currents ($_d$) from the ship transects in the radar domain.

a bias of -8.9 cm·s^{-1}. Similarly, the regression analysis for the along-shelf currents revealed a slope of 1.19 and a bias of 7.9 cm·s^{-1}, or about twice that in the 3-m bin comparisons. In both directions, current differences were again normally distributed falling within the 95% confidence limits.

V. Discussion

Progress in coastal oceanography has been generally slower to evolve than deep-water oceanography owing to its greater complexity both observationally and theoretically. Here, fronts, boundary layers, high-frequency internal waves, and turbulent processes occur together over short time and space scales. The VHF radar deployed in SFOMC demonstrated this high degree of current variability in the coastal ocean subjected to strong oceanic forcing mechanisms such as the Florida Current. The VHF mode of OSCR functioned well in July 1999, providing two-dimensional snapshots of a complex surface velocity structure at 250-m resolution over a continuous 29-d time/space series. This particular mode of OSCR is directly relevant to a broad spectrum of coastal marine activites, not the least of which is safe navigation into and out of ports and harbors and monitoring sewage effluent dispersion.

The results described here has provided a data set capable of resolving submesoscale surface processes and demonstrating linkages to subsurface ocean structure. Embedded within this surface current regime are unresolved subgrid scale processes that are usually parameterized in coastal ocean models. In this context, these data are potentially useful in exploiting the physics of these parameterizations for their eventual use in high-resolution ocean modeling. We believe that this technology has matured to a point where a coordinated engineering and scientific approach can be used to resolve complex coastal ocean processes from multiple platforms within the framework of networking coastal ocean observatories.

Central to this theme in South Florida is the intrusion of the Florida Current occuring over various time and space scales. That is, surface velocities changed by up to 2 m·s^{-1} over just a few hours, including submesoscale vortices and lobe-like structures with spatial scales of O(2 km). These fields suggest vorticites and divergences that scale as 3 to 4 f [19]. Coincident high-resolution mooring and ship data were in fact well correlated to observed surface processes. The level of agreement (correlations exceeding 0.8) between these platforms also provides ground truth to examine subsurface structure from five snapshots of AUV-based data [20], [25], [26]. This research effort is now in progress to understand aerial averaging of the radar signals relative to gridded AUV-measurements acquired over a few radar cells.

Noninvasive, surface radar observations offer a unique opportunity to assimilate data into linear and nonlinear numerical models. Such an approach offers a challenge over short time and space scales evident in the observed surface current fields [13]. This integrated level of data acquisition, analysis and modeling will provide background observations with an unprecedented level of detail for coastal ocean observing networks [23], [24] to examine physical characteristics over small scales. As these data are synthesized and analyzed, new insights will unfold into how a coastal ocean (narrow shelf) responds to FC forcing over an abrupt shelf break, including the surface current response to atmospheric forcing events (i.e., cold front passage) as observed in the April 2000 experiment and more recently in the May–June 2001 experiment.

Acknowledgment

The authors would like to thank J. Vasquez of the City of Hollywood Beach and J. Davis of Broward County Parks and Recreation for granting access to the property on the beach in Hollywood, L. Fisher and M. Taynton of the Florida Department of Environmental Protection and K. Moody of the Department of Forida Fish and Wildlife Commission for providing valuable assistance to the project, J. Carpenter for allowing access to her beach house for OSCR operations, Dr. R. Skinner and S. Leve for granting permission to use the beach at the J. U. Lloyd State Park, and Dr. B. Venezia at the US Navy South Florida Testing Facility for providing logistical support for our operations at the park. The authors further appreciate the efforts of Dr. B. Haus and Mr. J. Martinez in keeping the OSCR system maintained for field programs. Mr. J. Killingsworth participated in the experi-

ment as part of a summer internship at RSMAS. Insightful comments by the anonymous reviewers improved the manuscript.

REFERENCES

[1] D. D. Crombie, "Doppler spectrum of sea echo at 13.56 Mc. s^{-1}," *Nature*, vol. 175, no. 4459, pp. 681–682, 1955.
[2] R. H. Stewart and J. W. Joy, "HF radio measurements of surface currents," *Deep-Sea Res.*, vol. 21, pp. 1039–1049, 1974.
[3] K.-W. Gurgel, H.-H. Essen, and S. P. Kingsley, "High frequency radars: limitations and recent developments," *Coastal Eng.*, vol. 37, pp. 201–218, 1999.
[4] J. D. Paduan and H. C. Graber, "Introduction to high frequency radar: Reality and myth," *Oceanography*, vol. 10, no. 4, pp. 36–39, 1997.
[5] D. E. Barrick, "First order theory and analysis of MF/HF/VHF scatter from the sea," *IEEE Trans. Antennas Propagat.*, vol. 20, pp. 2–10, 1992.
[6] D. Prandle, "The fine-structure of nearshore tidal and residual circulations revealed by HF radar surface current measurements," *J. Phys. Oceanogr.*, vol. 17, no. 1, pp. 231–245, 1987.
[7] L. K. Shay, H. C. Graber, D. B. Ross, and R. D. Chapman, "Mesoscale ocean surface current structure detected by HF radar," *J. Atmos. Ocean. Technol.*, vol. 12, no. 4, pp. 881–900, 1995.
[8] K.-W. Gurgel, G. Antonischki, H.-H. Essen, and T. Schlick, "Wellen radar (WERA): a new ground wave HF radar for remote sensing," *Coastal Eng.*, vol. 37, pp. 219–234, 1999.
[9] B. J. Lipa and D. E. Barrick, "Least-squares methods for the extraction of surface currents from CODAR crossed loop data: Application at ARSLOE," *IEEE J. Ocean Eng.*, vol. OE-8, pp. 226–253, 4 1983.
[10] J. D. Paduan and L. K. Rosenfield, "Remotely sensed surface currents in Monterey Bay from shore-based HF radar (Coastal Ocean Dynamics Application Radar)," *J. Geophys. Res.*, vol. 101, no. 9, pp. 20 669–20 686, 1996.
[11] L. K. Shay, S. J. Lentz, H. C. Graber, and B. K. Haus, "Current structure variations detected by high frequency radar and vector measuring current meters," *J. Atmos. Oceanic. Technol.*, vol. 15, no. 1, pp. 237–256, 1998.
[12] L. K. Shay, T. N. Lee, E. J. Williams, H. C. Graber, and C. G. H. Rooth, "Effects of low frequency current variability on submesoscale near-inertial vortices," *J. Geophys. Res.*, vol. 103, no. 9, pp. 18 691–18 714, 1998.
[13] L. K. Shay, T. M. Cook, Z. Hallock, B. K. Haus, H. C. Graber, and J. Martinez, "The strength of the M_2 tide at the chesapeake bay mouth," *J. Phys. Oceanogr.*, vol. 31, no. 2, pp. 427–449, 2001.
[14] R. D. Chapman, L. K. Shay, H. C. Graber, J. B. Edson, A. Karachintsev, C. L. Trump, and D. B. Ross, "On the accuracy of HF radar surface current measurements: Intercomparisons with ship-based sensors," *J. Geophys. Res.*, vol. 102, no. 8, pp. 18 737–18 748, 1997.
[15] R. Weller and R. E. Davis, "A vector measuring current meter," *Deep-Sea Res.*, vol. 27A, pp. 575–582, 1980.
[16] P. Broche, J. C. Crochet, J. L. de Maistre, and P. Forget, "VHF radar for ocean surface current and sea state remote sensing," *Radio Sci.*, vol. 22, pp. 69–75, 1987.
[17] B. B. Balsley, A. C. Riddle, W. L. Ecklund, and D. A. Carter, "Sea surface currents in the equatorial pacific from VHF radar backscatter observations," *J. Atmos. Oceanic Technol.*, vol. 4, no. 3, pp. 530–535, 1987.
[18] L. K. Shay, T. M. Cook, B. K. Haus, J. Martinez, H. Peters, A. J. Mariano, P. E. An, S. Smith, A. Soloviev, R. Weisberg, and M. Luther, "VHF radar detects oceanic submesoscale vortex along the Florida coast," *EOS*, vol. 81, no. 19, pp. 209–213, 2000.
[19] H. Peters, L. K. Shay, A. J. Mariano, and T. M. Cook, "Current observations over a narrow shelf with large ambient vorticity," *J. Geophys. Res.*.
[20] N. J. Peters and R. A. Skop, "Measurements of ocean surface currents from a moving ship using VHF radar," *J. Atmos. Oceanic Tech.*, vol. 14, no. 3, pp. 676–694, 1997.
[21] H. C. Graber, B. K. Haus, R. D. Chapman, and L. K. Shay, "HF radar comparisons with moored estimates of current speed and direction Expected differences and implications," *J. Geophys. Res.*, vol. 102, no. 8, pp. 18 749–18 766, 1997.
[22] B. K. Haus, H. C. Graber, L. K. Shay, S. Nikolic, and J. Martinez, "1998: Ocean Surface Current Observations With HF Doppler Radar During the Cope-1 Experiment," University of Miami, Miami, FL, RSMAS Tech. Rep. 95-010.
[23] P. K. Kundu, "Ekman veering observed near the ocean bottom," *J. Phys. Oceanogr.*, vol. 6, no. 2, pp. 238–242, 1976.
[24] G. W. Marmorino, C. Y. Shen, C. L. Trump, N. Allan, F. Askari, D. B. Trizna, and L. K. Shay, "An occluded coastal ocean front," *J. Geophys. Res.*, vol. 103, no. 10, pp. 21 587–21 600, 1998.
[25] T. B. Curtin, J. G. Bellingham, J. Catipovic, and D. Webb, "Autonomous oceanographic sampling networks," *Oceanography*, vol. 6, no. 3, pp. 86–94, 1993.
[26] E. An, M. Dhanak, L. K. Shay, S. Smith, and J. VanLeer, "Coastal oceanography using autonomous underwater vehicles," *J. Atmos. Oceanogr. Tech.*, vol. 18, no. 2, pp. 215–234, 2001.

Lynn K. (Nick) Shay received the B.S. degree from the Florida Institute of Technology in 1976 and the M.S. and Ph.D. degrees from the US Naval Postgraduate School, Monterey, CA, in 1983 and 1987, respectively, all in physical oceanography.

He is currently an Associate Professor in the Division of Meteorology and Physical Oceanography at the University of Miami's Rosenstiel School of Marine and Atmospheric Science, Miami, FL. His research interests include: experimental and theoretical investigations of the ocean response and coupled air-sea interactions during strong atmospheric forcing events, the dynamics of ocean mixed layers and satellite and high-frequency radar studies to examine surface processes and their relationship to subsurface ocean structure. He has participated in several recent experiments including the ONR/NASA Surface Wave Dynamics Experiment, NSF/NOAA Coupled Ocean-Atmosphere Experiments in support of the United States Weather Research Program, ONR High Resolution Remote Sensing and 4-D Current Experiments. Recently, he lead the aircraft oceanographic component in the joint NSF/NOAA Eastern Pacific Investigation of Climate experiment. He has authored and co-authored over eighty peer-reviewed publications and reports.

Dr. Shay is a member of the American Meteorological Society and the American Geophysical Union.

c

Thomas M. Cook recieved the B.S. degree in atmospheric sciences from Rutgers University, New Brunswick, NJ, in 1992 and the M.S. degree in physical oceanography from Rosenstiel School of Marine and Atmospheric Science, University of Miami, Miami, FL, in 2000.

He is currently a Research Associate at the Rosenstiel School of Marine and Atmospheric Science specializing in nearshore and coastal oceanography, tidal circulation, and HF-radar measurement techniques.

Hartmut Peters received the B.S., M.S., and Ph.D. degrees in oceanography under the tutelage of Günther Dietrich, Drs. Lorenz Magaard and Gerold Siedler from Kiel University in Germany.

He held a postdoctoral position at the Applied Physics Laboratory, University of Washington, followed by a tenured position as Assistant Professor at the State University of New York at Stony Brook. He is now a Research Associate Professor at the Rosenstiel School of Marine and Atmospheric Science, University of Miami, Miami, FL. His interest is in the observation and modeling of small-scale processes in oceans and coastal waters, in turbulence and internal waves, and in their interactions with larger-scale currents.

Arthur J. Mariano was born in Bayonne, NJ. He received the B.S. degrees (with highest honors) in marine science and mathematics from Stockton State College and the Ph.D. degree in physical oceanography under the guidance of Dr. Tom Rossby from the University of Rhode Island, Providence.

He held a postdoctoral position with Dr. Allan Robinson at Harvard University, Cambridge, MA, and then with Dr. Otis Brown at the Rosenstiel School of Marine and Atmospheric Science, University of Miami, Miami, FL, where he is a Professor in the Division of Meteorology and Physical Oceanography. His research interests are data analysis and assimilation methods, ocean surface currents, meso-scale variability, and the analysis of ocean dynamics from Lagrangian observations.

Robert H. Weisberg received the B.S. degree in material science and engineering from Cornell University, Ithaca, NY, in 1969 and the M.S. and Ph.D. degrees in physical oceanography from the University of Rhode Island, Providence, in 1972 and 1975, respectively.

He is a Professor of Physical Oceanography in the College of Marine Science at University of South Florida. He is an experimental physical oceanographer with research interests in the circulation and air-sea interactions that occur in the equatorial regions of the world's oceans and on continental shelves and estuaries. He has authored or co-authored over 70 papersin professional journals. As director of the Ocean Circulation Group at USF, his present emphasis is on real-time and recording physical oceanographic measurements, analyses, and models of the west Florida continental shelf with applications to processes of societal importance.

Dr. Weisberg is a member of Sigma Xi, the American Geophysical Union, the American Meteorological Society, and The Oceanography Society.

P. Edgar An received the B.S.E.E. degree from the University of Mississippi in 1985, the M.S.E.E. degree from the University of New Hampshire in 1988, and the Ph.D. degree from the University of New Hampshire in 1991.

Since then he has been a Post-Doctoral Fellow in the Department of Aeronautics and Astronautics at the University of Southampton, U.K., working on the European Prometheus project. In 1994, he joined the Division of Ocean Engineering at Florida Atlantic University (FAU), Dania Beach, as a Visiting Faculty Member. His areas of interest are autonomous underwater vehicles, navigation, control, modeling and simulation, neuro-fuzzy systems. He became an assistant professor at FAU in 1995, and is currently an associate Professor at FAU. His publication record includes more than 70 journal and conference papers in these research areas. His areas of interest are autonomous underwater vehicles, control, navigation, modeling and simulation, system architecture, and design.

Dr. An is a recipient of the 1998 FAU Researcher of the Year award for the Assistant Professor level. He is a member of Sigma Xi.

Alexander Soloviev received the Diploma of Engineer from the Moscow Institute of Physics and Technology in 1976 and the Candidate of Sciences and Doctor of Sciences degrees from the former Soviet Academy of Sciences in 1979 and 1992, respectively.

He is an Associate Professor at the Nova Southeastern University's Oceanographic Center, Dania Beach, FL. He was previously a Visiting Scientist at the University of Hawaii and a Scientist in the two leading research institutions of the former Soviet Academy of Sciences: P.P. Shirshov Institute of Oceanology and A.M. Oboukhov Institute of Atmospheric Physics. His primary interest is upper ocean turbulent boundary layer and coastal circulation. He participated in several major air–sea interaction experiments (POLYMODE, JASIN, FGGE, TOGA COARE, GasEx-98) and is the author and co-author of more than 50 research articles.

Mark E. Luther received the B.S. degrees in physics and mathematics, the M.S. degree in physical oceanography, and the Ph.D. degree in physical oceanography from the University of North Carolina at Chapel Hill in 1976, 1980, and 1982, respectively.

He is an Associate Professor, University of South Florida College of Marine Science, St. Petersburg. His research involves the development of numerical models of ocean currents and processes and their application to various problems ranging from water quality in Tampa Bay to variability in large-scale ocean circulation and its relation to climate change. Most of his work involves combining real-time ocean observations with numerical models of ocean processes to provide "hindcasts" of past conditions, "nowcasts" of present conditions, or forecasts of future conditions. He presently serves on the U.S. Global Ocean Observing System (US-GOOS) Steering Committee and is the US National Delegate to the International Association for Physical Sciences of the Ocean (IAPSO).